LCT2-3L
(Late-News Paper)
Invited

Low-Driving-Voltage Liquid-Crystal-Lenses with High-Resistive Films

Marenori Kawamura

kawamura@gipc.akita-u.ac.jp
1-1 Tegata-gakunen machi, Akita city 010-8502

Keywords: Liquid crystal lens, focal length, phase retardation, circularly-hole patterned electrode, ring electrode

ABSTRACT

A three-dimensional numerical calculation for analyzing reorientation in liquid crystal (LC) directors and optical phase retardation in an LC lens, which exhibits a tunable lens property, is developed. The proposed LC lens design employs a circular electrode, ring electrodes, and a circular hole-patterned electrode employing a highly-resistive layer in a flat nematic cell.

1 Introduction

Liquid crystal (LC) materials have large optical anisotropies, that is, their optical properties parallel and perpendicular to the LC directors are quite different. The optical properties of LC materials are easily changed by electric fields. As a result, the LC materials are widely used in many kinds of electro-optical devices. The most well-known LC electro-optical devices are LC displays used in personal computer's monitors, smart phones and televisions. Besides LC displays, there are also used in LC electro-optical devices such as LC beam deflectors[1, 2] and LC modulators [3]. The other electro-optical devices as LC lenses [4-12] with a tunable focal length have been developed and the LC lenses are very promising for use in smart phone camera lenses, and microscope lenses and so on. Much researching interests have been attracted to these LC lenses. There are many methods for fabricating the LC lenses, and the electrically variable optical properties of the LC lens have been exhibited. Many LC lens structures have been reported, such as an LC lenses with electrodes coated on spherical lens surfaces [5], gradient index type LC lenses [6], polymer dispersed LC lenses [7], low-voltage-driving LC lens with both low aberrations and a wide focal range [8], LC lenses with severally-divided and circularly hole-patterned electrodes for steering and focusing a light beam. An LC lens exhibiting a conical lens property has been also developed [13]. Among them, some LC lenses have been used in imaging processing [14, 15], laser tweezers [16], zoom lens [17], and infrared imaging application [18].

In this paper, we propose an LC lens for controlling a lens property that has a realization of the low aberration lens profile. The LC lens has a circular upper electrode, multiple ring electrodes, a circularly hole-patterned electrode, and a bottom flat electrode. A highly-resistive thin film is deposited on the surface of an isolation film, which is coated on the upper electrodes. The lens property is demonstrated by applying voltages across the upper and bottom electrodes. The three-dimensional electric field distribution and the LC molecular orientations are numerically calculated using the finite element method. An LC lens exhibiting a lens property is fabricated, and optical retardation is experimentally demonstrated. The experimental results verify validity of the numerically calculated results.

2 LC lens structure and three-dimensional numerical calculation

Figures 1(a) and (b) show the LC lens model used in the three-dimensional numerical calculation. The diameter of the central circular electrode #1 is 0.3 mm, and the width of the ring electrodes #2–#5 is 1.1, 1.2, 1.3, 1.4 mm. The diameter of the circularly hole-patterned electrode, i.e., the lens region, is 14.8 mm. These electrodes are separated by 0.1 mm. The coordinate system used in this simulation is also shown, where the uniform bottom electrode is parallel to the *x*-*y* plane.

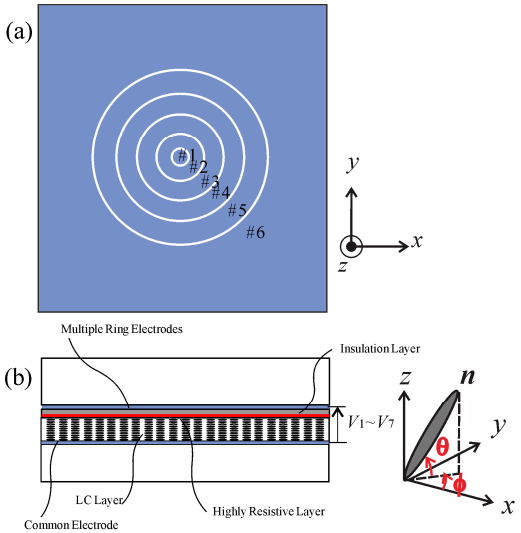

Fig. 1 Schematic diagram of LC lens

The 0.1-μm thick resistive layer with a sheet-resistance ρ_s and 5-μm thick insulation layer are stacked on the upper electrodes. A nematic LC material RDP87875 (DIC Co.) with a positive dielectric anisotropy was used. The LC material constants and cell parameters were used in the molecular orientation numerical calculations of the LC lens. The LC director on

the alignment layer of the glass substrate was aligned along the x-direction. With no applied voltages, the LC directors are homogeneously aligned, that is, the LC layer directors are nearly parallel to the surfaces of two alignment layers with a pretilt angle θ_s. Different voltages can be applied across the upper electrodes and bottom electrode. The unit director $\boldsymbol{n} = (n_x, n_y, n_z)$ is related to the z-axis, and it is described in the three dimensions by the following equations: $n_x = \cos\theta(z)\cos\phi(z)$, $n_y = \cos\theta(z)\sin\phi(z)$ and $n_z = \sin\theta(z)$, where $\theta(z)$ is the tilt angle and $\phi(z)$ is the azimuthal angle of the LC director in the z-direction. The elastic free-energy density of the LC system, which is stored in the electric field $\boldsymbol{E}$ can be expressed as follows: $f = \frac{1}{2}[k_{11}(\nabla \cdot \boldsymbol{n})^2 + k_{22}(\boldsymbol{n} \cdot \nabla \times \boldsymbol{n})^2 + k_{33}(\boldsymbol{n} \times \nabla \times \boldsymbol{n})^2] - \frac{1}{8\pi}\boldsymbol{D} \cdot \boldsymbol{E}$, where k_{11}, k_{22} and k_{33} are the splay, twist, and bend of the Frank elastic constants. The electric displacement in an LC system when an electric field is applied on the LC material is given as follows: $\boldsymbol{D} = \varepsilon_\perp \boldsymbol{E} + \Delta\varepsilon\,(\boldsymbol{n} \cdot \boldsymbol{E})^2$, where $\Delta\varepsilon = \varepsilon_{//} - \varepsilon_\perp$ is the dielectric anisotropy, $\varepsilon_{//}$ and $\varepsilon_\perp$ are the dielectric constants parallel and perpendicular to the local LC director. The threshold voltage $V_{th} = \pi\sqrt{k_{11}/(\varepsilon_0 \cdot \Delta\varepsilon)}$ is the voltage applied to an LC cell with a planar substrate LC cell when Frederick's transition occurs.

The electric field and reorientation of the LC directors were numerically calculated using the finite element method. The LC director profile in the LC layer at the equilibrium state can be determined by minimizing the total free energy. The equations in the equilibrium state of LCs can be obtained from the principle that the total free-energy density in the established state exhibits its minimum. The applied electric field rotates the directors to a tilt angle. The effective refractive index n'_e as a function of the tilt angle; θ experienced by an extraordinary light wave is given as follows: $n'_e = \frac{n_e n_o}{\sqrt{n_e^2 \sin^2(\theta) + n_o^2 \cos^2(\theta)}}$, where n_o and n_e are the ordinary and extraordinary refractive indices of the LC material. The optical phase retardation of a light incident to the LC layer can be calculated.

3 Results and discussion

The numerically calculated results of typical equipotential electric field distributions based on the LC material parameters and the cross-section for the voltages V_1 = 0.2 V, V_2 = 1.3 V, V_3 = 1.8 V, V_4 = 2.0 V, V_5 = 1.0 V and V_6 = 5.0 applied across the electrodes #1–#6 and the bottom electrode are shown in Fig. 2. The color bar indicates the electrical potential. The pretilt angle of the LC directors on the surface of the substrate is $\theta_s = 1°$. When a voltage is applied across the upper patterned electrodes and bottom flat electrode, a non-uniform electric field is formed in the LC layer due to the presence of a highly-resistive layer with a sheet-resistance $\rho_s = 10^6$ Ω/sq. The equipotential lines in the LC layer decrease gradually from the circular electrode #1 to the ring electrodes #2–#5 and the circularly hole-patterned electrode #6.

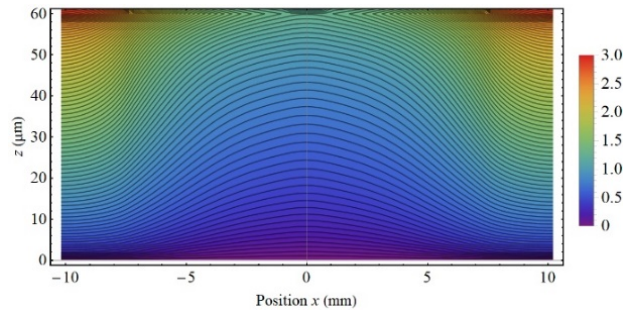

Fig. 2 Electric field distribution.

At the equilibrium state, both the LC directors and equipotential electric field distribution can be simultaneously calculated. Figure 3 shows the tilt angle distributions along the x-axis at y = 0 mm. The color bar indicates the tilt angle, whereas the blue and red colors indicate regions of small and large tilt angles, respectively. The orientations of the LC directors are determined by the elastic free-energy once exerted by the LC layer surfaces. The LC directors tend to reorient to align with the electric field until the electric torque is balanced by the elastic one. As the applied voltage increases, the LC molecules are forced to tilt in the rubbing plane. The rotating direction in which the tilt angle increases from 1° pretilt angle is defined as the positive direction. When the electric field is applied across the patterned electrodes of the upper substrate and the bottom uniform electrode, the LC directors rotate along the normal direction of the substrates.

Figure 4 shows the numerically calculated azimuthal angle distributions along the x-axis. The azimuthal angle along the x-axis is almost zero. The LC molecules near

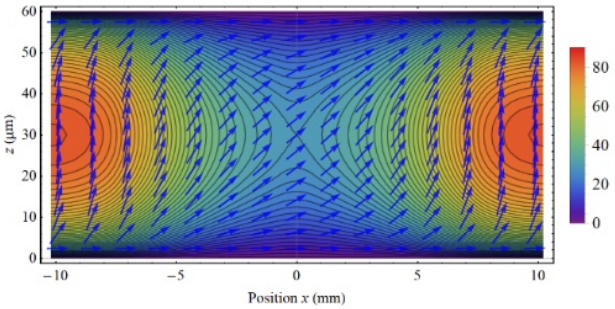

Fig. 3 Tilt angle distribution

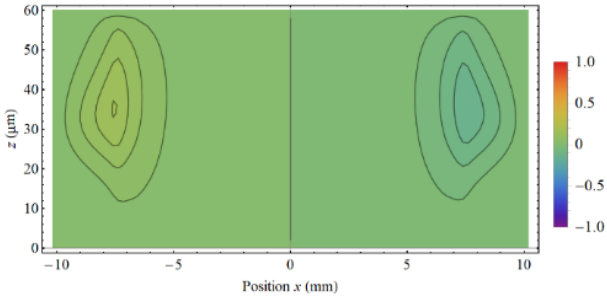

Fig. 4 Azimuthal angle distribution

both the ring electrodes #2– #5 and circularly hole-patterned electrode #6 of the upper substrate are twisted toward the perpendicular direction with respect to the initial alignment direction. This is due to the lateral electric fields induced by the ring electrodes and circularly hole-patterned electrode, while being tilted. The twisted angle is a function of the electric field strength when the voltages are applied across the ring electrode and hole-patterned electrode and the uniform electrode of the bottom substrate. The twisted angle of the LC molecules at the center of the circular electrode #1 is zero. In the LC layer bulk, the azimuthal angle and polar angle of the LC molecules depend on their spatial positions and the electric field strength.

Figure 5 shows the three-dimensional distribution cross-sectional distributions of the optical phase profile. The phase retardation can be calculated by using the tilt angles. The electric field in the LC layer exhibits its lowest value at the center and gradually increases from the center to the region around circularly hole-patterned electrode #6. The electric field profile is nearly symmetrical around the center. Due to the gradient distribution of the electric field, the tilt angle of the LC directors exhibits its lowest value at the center, and gradually increases from the center to the region around the edge of the circularly hole-patterned electrode. An axially symmetric non-uniform electric field distribution around the central line is formed in the LC layer. Therefore, the refractive index obtained from an incident extraordinary light wave exhibits its maximum value at the center and its lowest value at the circularly hole-patterned electrode. Thus, a parabolic spatial distribution of the effective refractive index can be obtained. The LC lens maps the planar wavefront of an incident light to a parabolic form, exactly as a convex glass lens does. The lens properties can be controlled by the applied voltages. The parabolic shape of the phase retardation can be obtained by controlling the applied voltages between the upper and the bottom electrodes.

Figure 6 shows the relationship between the root mean square (RMS) error and sheet-resistance of the highly-resistive film in the LC lens, where the voltages are applied across the patterned electrodes #1–#6 and the bottom electrode to preserve the parabolic phase retardation. The RMS error tends to decrease and increase with the sheet-resistance.

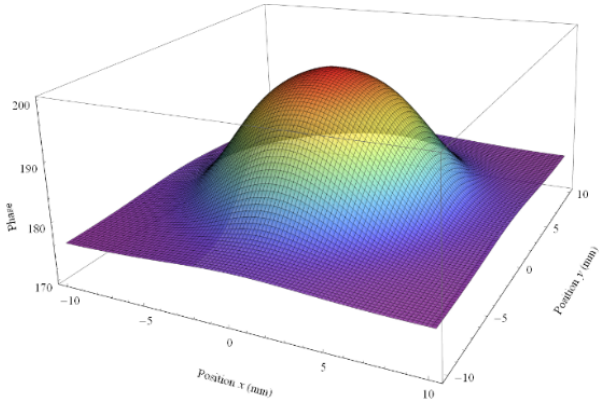

Fig. 5 Optical phase distribution.

Figure 7 shows the lens power in the LC lens as a function of the sheet-resistance. The lens power increases with the sheet-resistance and then lens power slowly decreases.

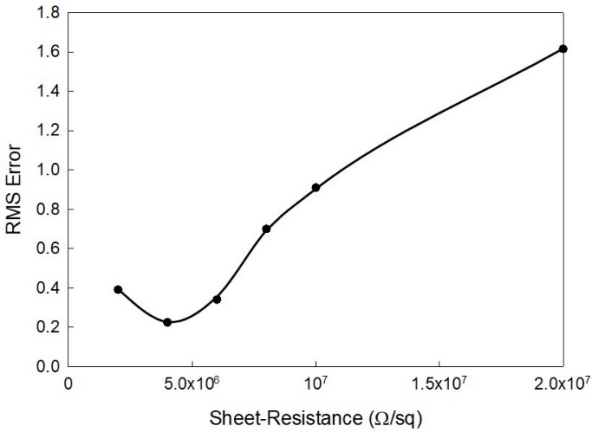

Fig. 6 RMS *vs* sheet-resistance.

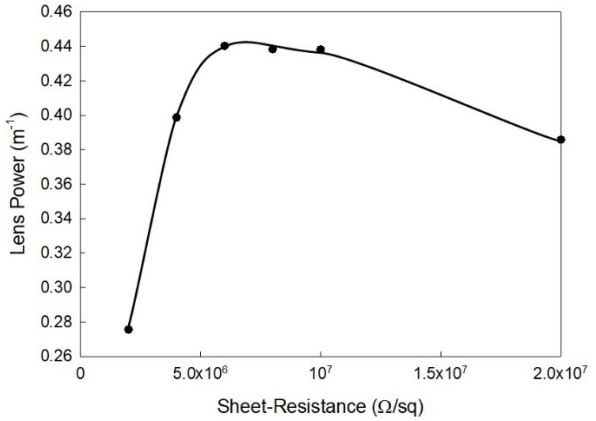

Fig. 7 Lens power *vs* sheet-resistance.

The LC lens structure used in the experiment was almost same as the lens structure fabricated for numerical calculation. In the experiment, when the voltages; V_1–V_6 shown in the numerical calculation were applied, the circular interference fringe pattern was obtained. The interference pattern shows the phase shift caused by the LC layer for an extraordinary wave. The phase retardation can be determined by counting the interference fringe, since its value between two neighboring interference fringes is 2π. A phase profile is obtained from the experimental results, and the cross-sectional distribution of the phase profile along the x-axis exhibits a bell-like shape. A close agreement between the experimental and numerically calculated results of the phase profiles of the LC lens with a parabolic lens property can be observed.

4 Conclusions

The three-dimensional LC molecular orientation in an LC lens, which exhibits a tunable lens property regarding the optical phase retardation, was investigated using the finite element method. The LC lens was implemented using a relatively small number of electrodes, i.e., a circular electrode, multiple ring electrodes and a bottom electrode of flat electrode with a highly-resistive layer. Three-dimensional distributions of the electric field, tilt angle, and azimuthal angle in the circularly hole-patterned region were simultaneously calculated. The optical property distribution is axially symmetric and exhibits a lens-like refractive index distribution.

5 Acknowledgment

The authors would like to thank Prof. Satoru Yoshimura for technical advice with the thin film fabrication. We also thank Prof. Susumu Sato for providing his expertise in the fundamental theory of a liquid crystal lenses. This work was partially supported by Grant-in-Aid for Scientific Research (C) JSPS KAKENHI, Grant Number JP17K06368 and JP20K04591, and Tateisi Science and Technology Foundation (2211008).

References

[1] A. F. Fray and D. Jones, "Large-angle beam deflector using liquid crystals," *Electron. Lett.,* vol. 11, no. 16, pp. 358 – 359, 1975, doi: 10.1049/el:19750273.

[2] S. Sato and A. Kikuchi, "Light deflection by nematic liquid-crystal cells," *OYOBUTURI,* vol. 45, no. 10, pp. 938-942, 1976, doi: 10.11470/oubutsu1932.45.938.

[3] S. Ohtaki, N. Murao, M. Ogasawara, and M. Iwasaki, "The applications of a liquid crystal panel for the 15 Gbyte optical disk systems," *Jpn J Appl Phys 1,* vol. 38, no. 3b, pp. 1744-1749, Mar 1999, doi: 10.1143/Jjap.38.1744.

[4] S. Sato, "Liquid-crystal lens-cells with variable focal length," *Jpn. J. Appl. Phys.,* vol. 18, no. 9, pp. 1679-1684, 1979/09 1979, doi: 10.1143/jjap.18.1679.

[5] B. Wang, M. Ye, M. Honma, T. Nose, and S. Sato, "Liquid crystal lens with spherical electrode," *Jpn. J. Appl. Phys.,* vol. 41, no. Part 2, No. 11A, pp. L1232-L1233, Nov 1 2002, doi: 10.1143/jjap.41.L1232.

[6] M. Ye and S. Sato, "Optical properties of liquid crystal lens of any size," *Jpn. J. Appl. Phys.,* vol. 41, no. Part 2, No. 5B, pp. L571-L573, 2002, doi: 10.1143/jjap.41.L571.

[7] V. V. Presnyakov and T. V. Galstian, "Electrically tunable polymer stabilized liquid-crystal lens," *Journal of Applied Physics,* vol. 97, no. 10, pp. 103101-103101-6, May 15 2005, doi: 10.1063/1.1896436.

[8] M. Ye, B. Wang, M. Yamaguchi, and S. Sato, "Reducing driving voltages for liquid crystal lens using weakly conductive thin film," *Jpn. J. Appl. Phys.,* vol. 47, no. 6 PART 1, pp. 4597-4599, 2008, doi: 10.1143/JJAP.47.4597.

[9] H. Yu, G. Zhou, H. M. Leung, and F. S. Chau, "Tunable liquid-filled lens integrated with aspherical surface for spherical aberration compensation," *Opt Express,* vol. 18, no. 10, pp. 9945-54, May 10 2010, doi: 10.1364/OE.18.009945.

[10] H.-C. Lin and Y.-H. Lin, "An electrically tunable focusing liquid crystal lens with a built-in planar polymeric lens," *Applied Physics Letters,* vol. 98, no. 8, 2011, doi: 10.1063/1.3559622.

[11] T. Galstian *et al.*, "High optical quality electrically variable liquid crystal lens using an additional floating electrode," *Opt Lett,* vol. 41, no. 14, pp. 3265-8, Jul 15 2016, doi: 10.1364/OL.41.003265.

[12] Y. H. Hsu, B. Y. Chen, and C. R. Sheu, "Improvement of hole-patterned electrode liquid crystal lens by coplanar inner ring electrode," *IEEE Photonics Technol Lett,* vol. 31, no. 20, pp. 1627-1630, Oct 2019, doi: 10.1109/lpt.2019.2939268.

[13] M. Kawamura, Y. Ichimura, and T. Sugawara, "Liquid crystal lens with tunable conical lens properties," *Jpn. J. Appl. Phys.,* vol. 60, no. 4, p. 6, 2021, doi: 10.35848/1347-4065/abed63.

[14] M. Ye, B. Wang, M. Kawamura, and S. Sato, "Image formation using liquid crystal lens," *Jpn J Appl Phys Part 1 Regul Pap Short Note Rev Pap,* vol. 46, no. 10 A, pp. 6776-6777, 2007, doi: 10.1143/JJAP.46.6776.

[15] M. Kawamura, E. Yumoto, and S. Ishikuro, "Three-dimensional imaging system by using a liquid crystal lens," *IEEE Xplore,* 2012, doi: 10.1109/ISOT.2012.6403232.

[16] M. Kawamura, M. Ye, and S. Sato, "Optical particle manipulation using an LC device with eight-divided circularly hole-patterned electrodes," *Opt Express,* vol. 16, no. 14, pp. 10059-65, Jul 7 2008, doi: 10.1364/oe.16.010059.

[17] M. Ye, M. Noguchi, B. Wang, and S. Sato, "Zoom lens system without moving elements realised using liquid crystal lenses," *Electron. Lett.,* vol. 45, no. 12, 2009, doi: 10.1049/el.2009.0840.

[18] M. Kawamura, S. Sato, and S. Sato, "Electrically tunable liquid-crystal optical and imaging devices operating in the infrared wavelength range of 10 μm band," *Jpn. J. Appl. Phys.,* vol. 58, no. 8, 2019, doi: 10.7567/1347-4065/ab2c2e.